Journal of Materials Chemistry A

Accepted Manuscript

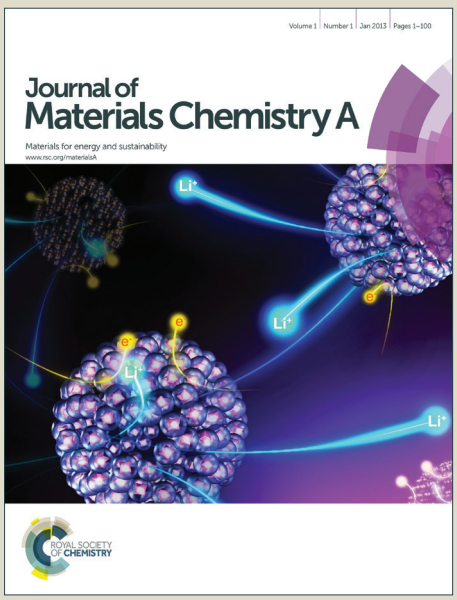

ROYAL SOCIETY OF CHEMISTRY

www.rsc.org/materialsA

A comprehensive study on the effect of preparation methods for Au-core@shell silica materials in room temperature oxidative amide formation

Jiale Huang,[a] Mingyu Zhang,[a] Jing Wang,[b] Xijun Hu,[a] Rafael Luque,[a, c] and Frank L. Y. Lam [a]*

[a] Department of Chemical and Biomolecular Engineering, Hong Kong University of Science and Technology, Clear Water Bay, Hong Kong, P. R. China, E-mail: kefrank@ust.hk , [b] Department of Chemical and Biochemical Engineering, College of Chemistry and Chemical Engineering, Xiamen University, Xiamen, 361005, P. R. China, [c] Departamento de Química Orgánica, Universidad de Córdoba, Campus Universitario de Rabanales, Edificio Marie Curie (C3), Córdoba, Spain, Email: q62alsor@uco.es, rafaluque@ust.hk

Abstract

Core-shell silica comprising mesoporous SiO_2 shell and solid SiO_2 core (SiO_2@mSiO_2) was utilized as catalytic support to prepare highly active and efficient Au/SiO_2@mSiO_2 catalysts for room temperature catalysis. Results showed that the mesoporous shell significantly contributed to the high surface area of SiO_2@mSiO_2. Au nanocatalysts prepared by different methods (impregnation, IM and deposition-precipitation-DP) exhibited remarkably different structural properties. Au/SiO_2@mSiO_2 catalysts exhibited excellent catalytic activity and high stability. Conversion could reach ca. 54% in the amidation of benzaldehyde and morpholine, with a complete selectivity to the target amide product at room temperature.

Keywords

Heterogeneous catalyst, gold nanoparticles, core-shell silica, direct amidation.

1. Introduction

Noble metal catalysts play an important role in the refining, petrochemical, environmental protection and other fields owing to their superior catalytic performance. Gold was long considered to be chemically inert as compared with other precious metals, therefore with restricted catalytic applications in the past[1-4]. Haruta *et al*. reported for the first time the remarkable catalytic activity of highly dispersed gold nanoparticles (AuNPs) supported over transition metal oxides for low-temperature CO oxidation in the late 80s.[4] As a result, the traditional concept of catalytically inactive gold was changed [1, 5-7]. Nanocatalysis has become one of the cutting-edge subjects in the field with the rapid development of nanotechnology[6, 7], with Au NPs proven to be catalytically active for many reactions including oxidation of alcohols[8, 9], epoxidation of propylene[10-12] and hydrogenations[13, 14].

The particle size of both Au NPs and the catalytic support are two important aspects to be considered in the preparation of supported nano-gold catalysts. Size control of AuNPs relies on the synthetic methods. Impregnation (IM) and deposition-precipitation (DP) methods are usually employed to prepare supported nano-gold catalysts[7]. IM has been traditionally employed to prepare supported noble metal catalysts. However, a low controllability of reaction parameters renders nanomaterials with wider size distribution of nanoparticles as well as larger nanoparticle sizes upon calcination at higher temperatures. The use of porous supports with different structures may improve some disadvantages of the IM method which is still far from being ideal for NP deposition. Comparatively, DP has been particularly useful for the synthesis of gold nanomaterials as it can lead to fine AuNPs over a wide range of supports with essentially superior catalytic activities[7].

The use of nano-gold catalysts in fine chemical synthesis has attracted much attention in recent years[7]. As one of morpholine derivatives, 4-benzoylmorpholine is a valuable intermediate in the

synthesis of pharmaceuticals[15]. 4-benzoylmorpholine can be produced from benzaldehyde and morpholine via gold-catalyzed amide formation using a simple Au/SiO_2 catalyst under laser-irradiation[15]. By selectively activating the plasmonic AuNPs, the laser energy was absorbed and converted into heat which drives the reaction to completion in a few hours. Common silica nanoparticles were used as support for AuNPs.

In the past decade, considerable efforts have been devoted to the design and application of heterogeneous nanocatalysts by incorporating new nanostructured materials[16]. Core-shell materials which can integrate different functional components into one unit have been received much attention in recent years[17]. A significant advance for the preparation of silica particles was reported by Stöber *et al*., which described the controlled growth of monodisperse silica spheres in the micron size range[18]. The Stöber method was consequently extended to design mesoporous SiO_2 and TiO_2 shells for uniform multifunctional core–shell structures[17]. The utilization of core-shell materials has several advantages as catalytic support since noble metal nanoparticles can be entrapped and stabilized in the porous shells. The effect of confined metal nanoparticles may give rise to unique catalytic activity, while an excellent stability and durability of the catalytic systems can be achieved.

In view of the possibilities of core-shell silica materials as support of metal nanoparticles, we report herein the design of mesoporous SiO_2 shell and solid SiO_2 core (SiO_2@mSiO_2) core-shell nanomaterials as catalytic support for the deposition of Au NPs towards advanced heterogeneous catalysts at room temperature (RT). The oxidative amidation reaction between benzaldehyde and morpholine was selected as test reaction at RT (Scheme 1). Au/SiO_2@mSiO_2 catalysts exhibited excellent catalytic activity and a complete selectivity to target product 4-benzoylmorpholine. The effect of synthesis methods (IM and DP) on the distribution of AuNPs over the support, their

nanoparticle size and catalytic performance were comparatively investigated.

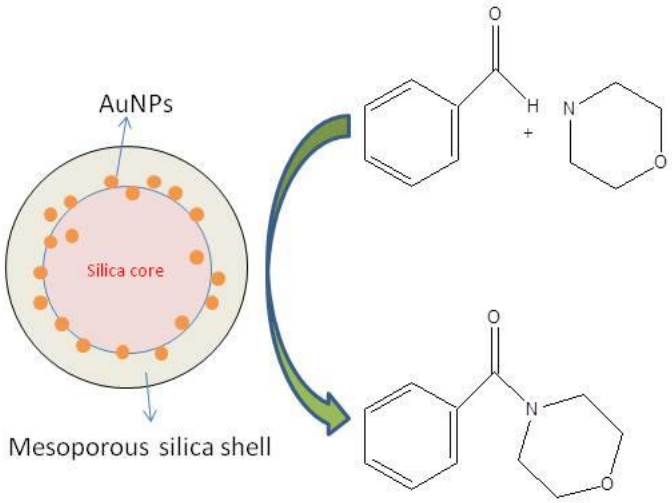

Scheme 1 Au-core@shell silica materials for room temperature oxidative amide formation

2. Experimental

2.1 Materials

Benzaldehyde (C_7H_8O, ≥99%), tetrahydrofuran (C_4H_8O, THF, ≥99.9%), morpholine (C_4H_9NO, ≥99.0%), tetraethyl orthosilicate (TEOS, 98%), aqueous hydrogen peroxide (H_2O_2, 30%), cetyltrimethyl ammonium bromide (CTAB), ammonium nitrate (NH_4NO_3, ≥98%), potassium carbonate (K_2CO_3, 99%) and gold (III) chloride trihydrate ($HAuCl_4$, 99.9+%) were purchased from Sigma-Aldrich Co. Ltd. Ammonia solution ($NH_3 \cdot H_2O$, 0.89 g/cm^3), ethanol (C_2H_5OH, 96%vol) and potassium hydroxide (KOH, 85.0%) were purchased from VWR International Ltd. 4-benzoyl morpholine ($C_{11}H_{13}NO_2$, 98+%) was purchased from International laboratory USA.

2.2. Preparation of core-shell SiO_2@mSiO_2

Aqueous $NH_3 \cdot H_2O$ of 20 mL was added to a 90 vol.% ethanol solution (200 mL) in a 500 mL flask under constant stirring (500 rpm). After 10 min stirring, 20 mL TEOS was added and the

mixture was left stirring for 24 h. The mixture was then centrifuged at 6000 rpm for 5 min and washed using 10 mL ethanol (3 times). The obtained product (core SiO_2) was dried at 60ºC.

50 mL ethanol, 100 mL deionized water and 2 mL $NH_3 \cdot H_2O$ were mixed in a 500 mL flask. 0.6 g core SiO_2 (prepared in the previous step) was added to the solution and subjected to ultrasounds for 20 min to obtain a better dispersed solution. 0.2 g cetyltrimethylammonium bromide (CTAB) was then dissolved in the solution under constant stirring (750 rpm), and the mixture was stirred for 12h. 0.32 mL TEOS was then added and reacted for an additional 12 h. The final solution was then centrifuged and washed using ethanol (3 times). The obtained white solid was dried at 70ºC and then calcined at 500ºC for 3 h. The material was denoted as $SiO_2@mSiO_2$.

2.3. Preparation of $Au/SiO_2@mSiO_2$

$Au/SiO_2@mSiO_2$ with Au loading of 2% was prepared using conventional IM and DP methods. The IM method consisted in the preparation of an aqueous 0.5 M $HAuCl_4$ solution (0.6 mL) which was subsequently added dropwise to 3 g $SiO_2@mSiO_2$ while stirring. The final yellow solid was dried at 90ºC, reduced and calcined at different temperatures (300~500ºC) in pure hydrogen and air flow, respectively. The catalysts were denoted as $Au/SiO_2@mSiO_2$(IM)-x-y, where x and y stand for the calcination atmosphere and temperature, respectively.

In the DP method[19], 3 g $SiO_2@mSiO_2$ was mixed with 50 mL H_2O in a 250 mL flask. Then, 0.609 mL 0.5 M aqueous solution of $HAuCl_4$ was added to the mixture at 60ºC under constant stirring for 30 min. The pH was then adjusted to 9-10 by adding aqueous $NH_3 \cdot H_2O$ and the solution was left stirring for 24 h. The final mixture was then filtered off and washed by deionized water (3 times) and dried at 60ºC for 12 h. The obtained yellow solid was calcined at 3 different temperatures (300~500ºC) in pure hydrogen and air flow, respectively. The catalysts were denoted as $Au/SiO_2@mSiO_2$(DP)-x-y,

where x and y similarly stand for calcination atmosphere and temperature, respectively.

2.4 Characterization of the catalysts

BET Surface areas were measured in a Micromeritics Tristar system (Tristar 3000). Before measurements, samples were outgassed at 300ºC for 3 h. X-ray diffraction (XRD) measurements were performed on an X'Pert Pro (PAnalytical) X-ray Diffractometer. Transmission electron microscopy (TEM) images of the samples were obtained on a JEM 2010F (JEOL) microscope and Phillips Analytical FEI Tecnai 30 microscope. Size distribution of SiO_2 core and AuNPs, and thickness distribution of SiO_2 shells were measured using a previously reported method[11].

XPS measurements were performed with a Kratos Analytical AXIS 165 electron spectrometer using a monochromated AlKα X-ray source run at 100 W. Survey scans were taken with a 1.0 eV step and 80 eV analyzer pass energy while the high resolution regional spectra were recorded with a 0.1 eV step and 20 eV pass energy. The base pressure was typically 1×10^{-9} Torr.

2.5 Catalytic reactions

The oxidative amidation between benzaldehyde and morpholine were conducted at room temperature. In a typical experiment, 0.2 mL benzaldehyde and 0.2 mL morpholine were mixed in 19 mL THF in a 50 mL flask. 0.01 g KOH, 0.025 g catalyst and 1 mL H_2O_2 were added to the solution under constant stirring (500 rpm). Samples were filtered and analyzed using a gas chromatography (GC) Bruker 430 fitted with a PTE-5 capillary column and FID detector. Response factors of the reaction products were determined with respect to the starting materials from GC analysis.

3. Results and Discussion

Figure 1 shows TEM images of SiO_2 particles of spherical morphology prepared by the Stöber

method. Histograms of their size distribution (Figure S1, Supplementary Information) pointed to the presence of NP sizes in the range of 360 to 430 nm, with a mean size of 388±15 nm. SiO_2 particles were further coated with the SiO_2 shell containing CTAB molecules, which resulted in a mesoporous SiO_2 shell upon surfactant removal after calcination at 500 ^oC. Figure 2a and 2b shows representative TEM images of resulting SiO_2@mSiO_2 materials. Single SiO_2@mSiO_2 particle comprise a solid core and a mesoporous shell. The histogram of the shell thickness distribution (Figure S2, ESI) indicates a ca. 25.8±2.4 nm thickness of the mesoporous shell.

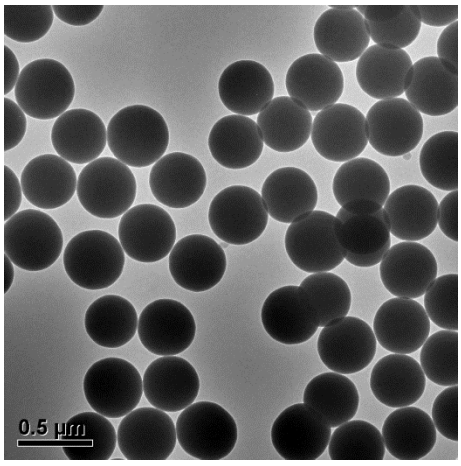

Figure 1 (a) TEM image of SiO_2 particles

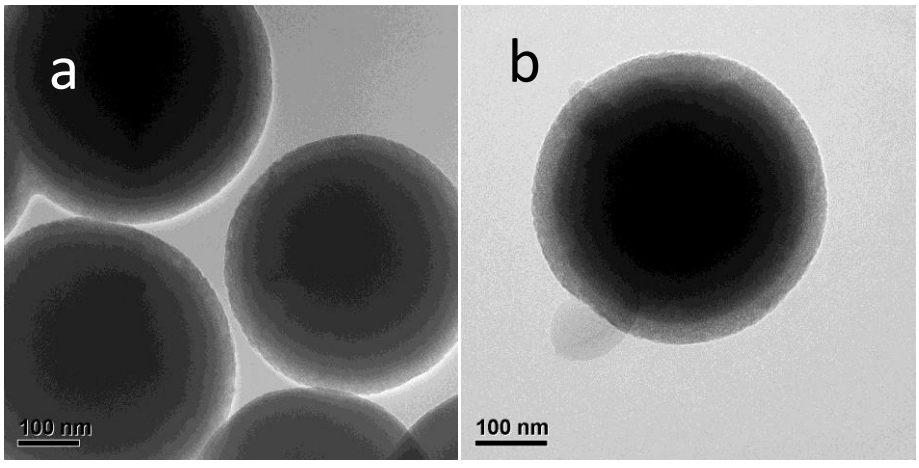

Figure 2 (a-b) TEM images of SiO_2@mSiO_2 particles

Table 1 summarises key textural properties of the materials synthesized in this work. The solid silica core exhibited a very low surface area, which was significantly improved upon generation of

the mesoporous shell (144 m^2 g^{-1}, Table 1). The pore diameter and volume of the mesoporous shell were about 1.50 nm and 0.107 cm^3 g^{-1}, respectively.

Table 1. Textural properties of synthesized materials

Sample	S_{BET} ($m^2 \cdot g^{-1}$)	Pore diameter[a] (nm)	Pore volume[b] ($cm^3 \cdot g^{-1}$)
SiO_2	<15	2.4	0.03
Core-shell SiO_2	144	1.5	0.11
Au/SiO_2@mSiO_2(IM)-H_2-300	169	1.4	0.10
Au/SiO_2@mSiO_2(IM)-H_2-400	113	1.7	0.09
Au/SiO_2@mSiO_2(IM)-H_2-500	153	1.4	0.10
Au/SiO_2@mSiO_2(IM)-Air-300	129	1.4	0.09
Au/SiO_2@mSiO_2(IM)-Air-400	142	1.4	0.09
Au/SiO_2@mSiO_2(IM)-Air-500	127	1.5	0.09
Au/SiO_2@mSiO_2(DP)-H_2-300	54	3.1	0.09
Au/SiO_2@mSiO_2(DP)-H_2-400	74	2.6	0.12
Au/SiO_2@mSiO_2(DP)-H_2-500	33	6.3	0.07
Au/SiO_2@mSiO_2(DP)-Air-300	36	9.4	0.05
Au/SiO_2@mSiO_2(DP)-Air-400	51	3.7	0.08
Au/SiO_2@mSiO_2(DP)-Air-500	33	8.9	0.05

[a] Calculated from the desorption branch by using the BJH model.[b] Calculated from the volume adsorbed of P/P_0 at 0.99.

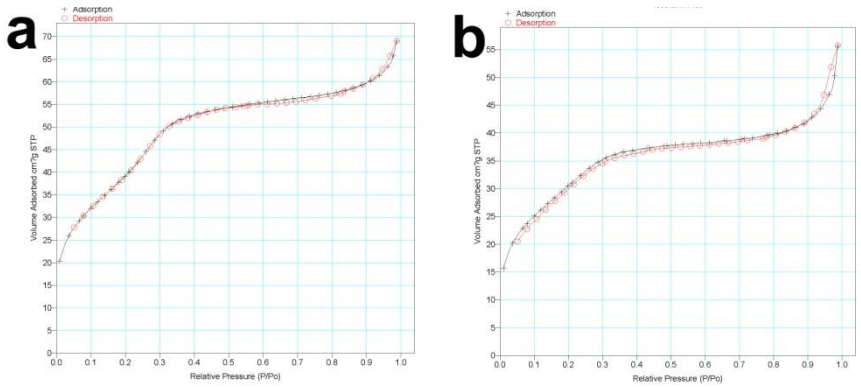

Figure 3 Nitrogen adsorption–desorption isotherms of (a) SiO_2@mSiO_2 and (b) Au/SiO_2@mSiO_2

The volume of the shell only accounts for ca. 30% of the total volume of individual SiO_2@mSiO_2 particles. SiO_2@mSiO_2 materials exhibited a typical type IV, characteristic of mesoporous materials (Figure 3a). The mesoporous structure was preserved upon Au incorporation as suggested by the almost identical isotherm profile observed for Au/SiO_2@mSiO_2 materials (Figure 3b). XRD patterns of as-prepared SiO_2@mSiO_2 (Figure 4, bottom) pointed out its inherent amorphous nature with the presence of a broad diffraction line at 2θ=23, typical of amorphous silicates[20]. In contrast, various sharp diffraction lines can be distinctly observed in the XRD patterns of Au/SiO_2@mSiO_2, which can be indexed to face-centered cubic structure of gold[21]. The XRD patterns thus clearly show that the Au NPs on SiO_2@mSiO_2 are highly crystalline.

The prepared catalysts of SiO_2@mSiO_2 and Au/SiO_2@mSiO_2 materials without pretreatment were directly characterized by X-Ray Photoelectron Spectroscopy (XPS) to study their surface properties. Figure 5a and Figure 5b shows Si2p and O1s spectra from SiO_2@mSiO_2 and Au/SiO_2@mSiO_2, respectively, showing typical spectra of silica materials. Figure 6 depicts the Au4f XP spectrum of Au/SiO_2@mSiO_2. The spectrum showed an intense Au 4f7/2 signal at 83.9 eV, indicating the presence of zero-valent Au in the material[22]. The mass percentage of each element in SiO_2@mSiO_2 and Au/SiO_2@mSiO_2 was measured by XPS and summarized in Table 2. Au content of

catalysts prepared via DP were remarkably larger (5 to 10 times superior) as compared to those of materials prepared via IM. A larger concentration of Au nanoparticles may be generated within the mesopore shell of SiO_2@mSiO_2, thus leading to a lower quantifiable Au content on the surface of the support.

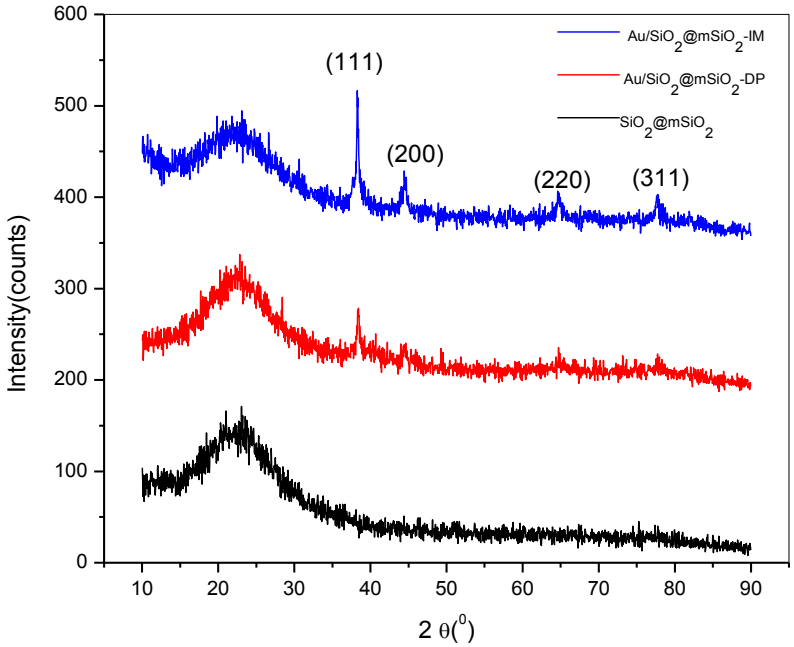

Figure 4 XRD patterns of SiO_2@mSiO_2 and Au/SiO_2@mSiO_2 catalysts

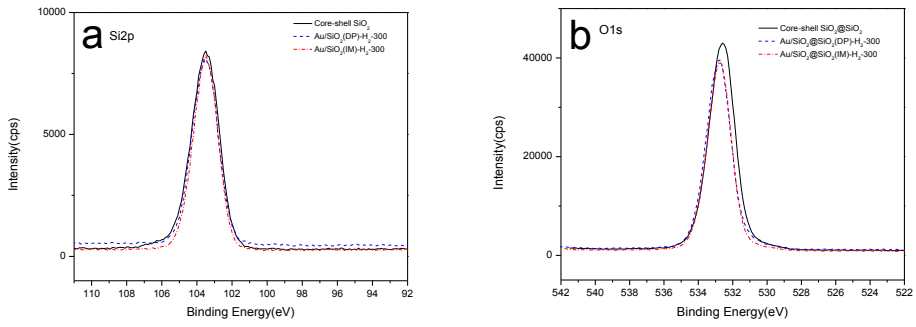

Figure 5 (a) Si2p and (b) O1s XP spectra of SiO_2@mSiO_2 (continuous line) and Au/SiO_2@mSiO_2 (discontinuous line).

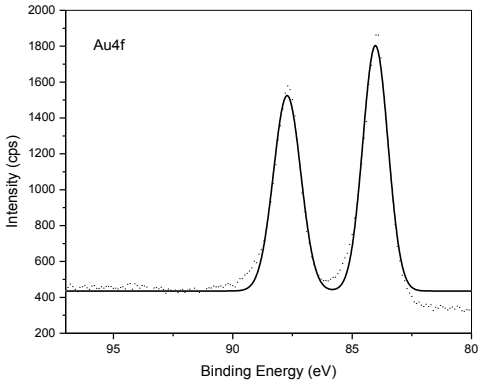

Figure 6 Au4f XP spectrum of $Au/SiO_2@mSiO_2$.

Table 2. Mass percentage of elements in different $SiO_2@mSiO_2$ materials

Support/catalysts	O	Si	C	Au
Core-shell $SiO_2@mSiO_2$	54	43	3	-
$Au/SiO_2@mSiO_2$(DP)-H_2-300	51	40	4.4	4.0
$Au/SiO_2@mSiO_2$(DP)-H_2-400	51	42	1.8	5.2
$Au/SiO_2@mSiO_2$(DP)-Air-300	53	43	2.2	2.1
$Au/SiO_2@mSiO_2$(IM)-H_2-300	54	43	2.3	0.6
$Au/SiO_2@mSiO_2$(IM)-Air-300	53	44	2.1	0.5

Au incorporation was found to have an effect on the textural properties of $SiO_2@mSiO_2$, particularly under DP conditions (Table 1). Au/ $SiO_2@mSiO_2$ materials prepared via IM did not exhibit any significant deterioration in textural properties (surface area, pore volume or diameter). In contrast, materials prepared using the DP method exhibited a remarkably decreased surface area and greatly increased pore diameters. Due to the precipitation of Au precursor on the shell layer under DP conditions, the mesoporous shell may have collapse to some extent accounting for the observed differences in the materials.

TEM images of $Au/SiO_2@mSiO_2$ catalysts prepared at different calcination conditions via IM and DP have been included in Figures 7 to 9. Starting with materials prepared under IM conditions, Au nanoparticles were found to be homogeneously distributed in the shell of the support (Figure 7).

The core-shell structured feature was slightly changed upon Au incorporation. Au NPs size distribution histograms (Figure S3, Supplementary Information) indicate that Au nanoparticles possessed sizes in the 2 to 14 nm range. Their mean size and size distribution were not significantly affected by increasing the calcination temperature from 300 to 400 ^{o}C. However, their mean size was larger, with a wider size distribution upon further increasing calcination temperatures (from 400 to 500 ^{o}C). As expected, AuNPs tended to aggregate at higher calcination temperatures. TEM images of DP prepared Au/SiO_2@mSiO_2 catalysts are included in Figures 8 and 9. A certain damage induced in the mesoporous shell can be clearly visualized in all cases upon Au incorporation. Furthermore, the formed Au nanoparticles were larger (Figure S4 and S5, Supplementary Information) as compared to those prepared by the IM method. These findings are in good agreement with the observed changes in textural properties (e.g. reduction in surface area as well as increase in mesopore diameter) which seem to be due to Au incorporation via DP.

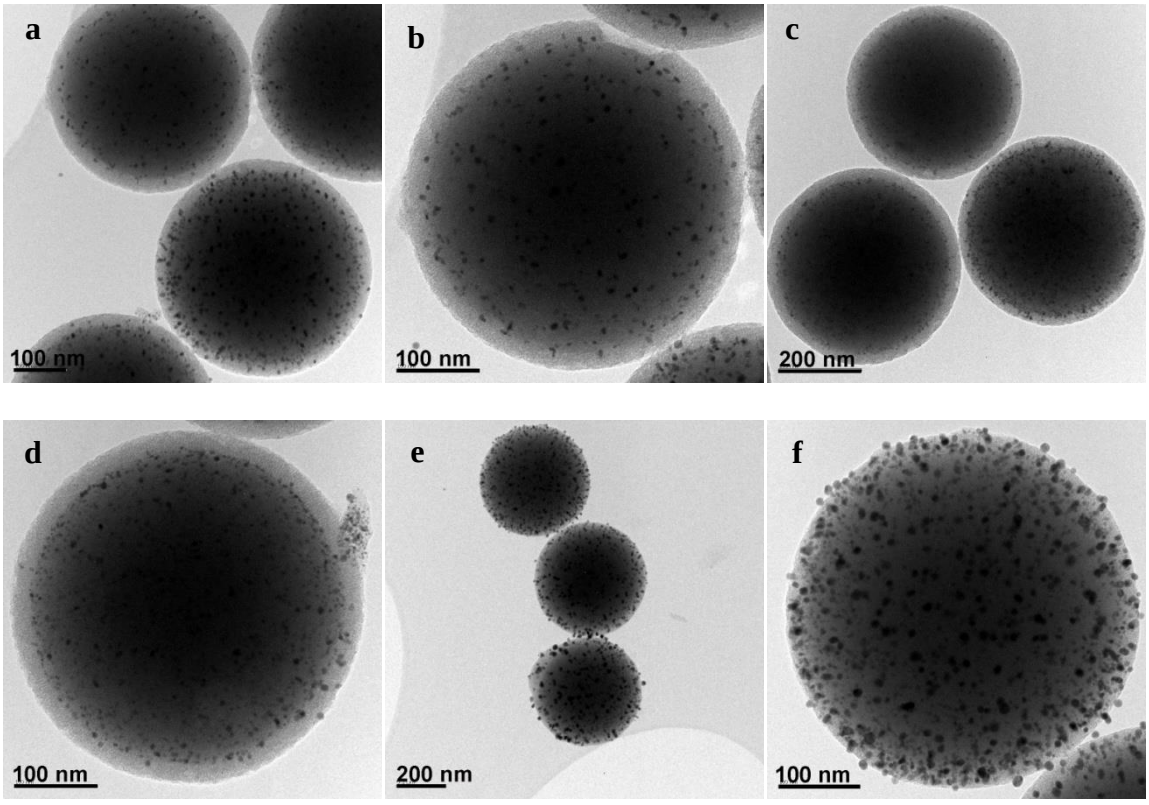

Figure 7 TEM images of (a) Au/SiO_2@mSiO_2(IM)-H_2-300, (b) Au/SiO_2@mSiO_2(IM)-H_2-400 and (c)

Au/SiO_2@mSiO_2(IM)-H_2-500 catalysts

Prior to Au immobilization, the size of Au nanoparticles are larger than the original diameter of the mesopores. It was easy for the Au precursor solution to penetrate into the mesopores of SiO_2@mSiO_2. During the calcination, the growth of the Au nanoparticles led to in-situ expansion of the mesopores. However, they were still stabilized by the mesoporous shell.

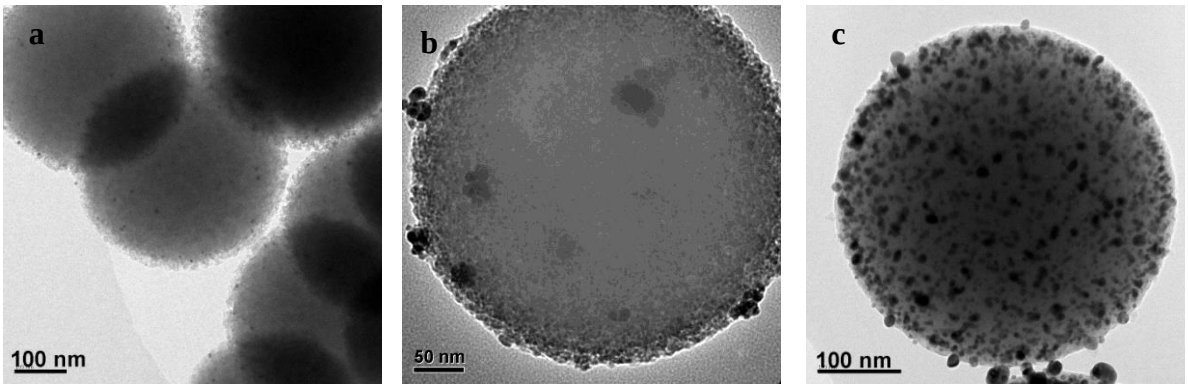

Figure 8 TEM images of (a) Au/SiO_2@mSiO_2(DP)-H_2-300, (b) Au/SiO_2@mSiO_2(DP)-H_2-400 and (c) Au/SiO_2@mSiO_2(DP)-H_2-500 catalysts

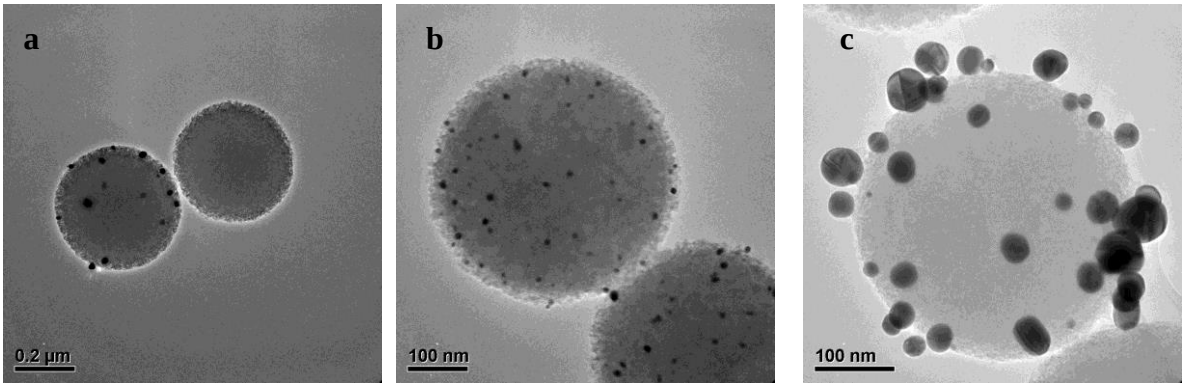

Figure 9 TEM images of (a) Au/SiO_2@mSiO_2(DP)-air-300, (b) Au/SiO_2@mSiO_2(DP)-air-400 and (c) Au/SiO_2@mSiO_2(DP)-air-500 catalysts

Catalytic performance of Au/SiO_2@mSiO_2

The catalytic performance of Au/SiO_2@mSiO_2 materials was tested in the reaction of benzaldehyde and morpholine to produce 4-benzoylmorpholine at room temperature (Scheme 1).

Generally good conversions (>50%) could be obtained for the different supported Au NP materials. The selectivity to the target product was 100%, with no detected by-products under the investigated conditions. The effect of calcination temperature, reaction time and catalyst amount in the catalytic activity of Au-systems was also investigated, with interesting differences observed between DP and IM prepared catalysts (Table 3). Au-SiO_2@mSiO_2 materials prepared via DP (calcined in H_2 amosphere) exhibited a high activity (55%, 4h reaction) for the material at 300 ºC, which decreased upon increasing temperature of calcination to 400 and 500 ºC (Table 3). These findings correlate well a decrease in catalytic activity with an increase in Au NPs sizes as observed in TEM images (Figure 8). The catalytic behavior of IM Au-SiO_2@mSiO_2 materials was significantly different (Table 3). Morpholine conversion was essentially identical irrespective of the calcination temperature in the materials. In the case of IM Au-SiO_2@mSiO_2, the observed results can be correlated to the confination of AuNPs within the mesopore shell (as opposed to Au NPs present on the supports surface in the DP method), which prevented a significant NP aggregation even at higher calcination temperatures. It can be also figured out that the TOF depended on the AuNP size. For either DP or IM method, the catalysts containing smaller size AuNPs (Au/SiO_2@mSiO_2(DP)-H_2-300 and Au/SiO2@mSiO_2(IM)-H_2-300) gave rise to improved reaction rates.

Table 3. Catalytic performance of Au/SiO_2@mSiO_2 materials[a]

Catalysts	AuNP Size/nm	Catalyst amount/g	H_2O_2 amount/mL	Reaction time/h	Morpholine conversion/%	TOF/h^{-1}
Au/SiO_2@mSiO_2(DP)-H_2-300	8.5±1.6	0.025	1.0	4	55.2	126
Au/SiO_2@mSiO_2(DP)-H_2-400	12.3±1.9	0.025	1.0	4	37.8	86
Au/SiO_2@mSiO_2(DP)-H_2-500	10.0±1.7	0.025	1.0	4	35.8	82
Au/SiO_2@mSiO_2(IM)-H_2-300	7.1±1.1	0.025	1.0	4	53.9	123
Au/SiO_2@mSiO_2(IM)-H_2-400	7.1±0.9	0.025	1.0	4	54.3	124
Au/SiO_2@mSiO_2(IM)-H_2-500	10.3±1.5	0.025	1.0	4	47.9	109
Au/SiO_2@mSiO_2(IM)-H_2-300	7.1±1.1	0.015	1.0	4	48.7	185
Au/SiO_2@mSiO_2(IM)-H_2-300	7.1±1.1	0.05	1.0	4	55.3	63
Au/SiO_2@mSiO_2(IM)-H_2-300	7.1±1.1	0.025	1.0	1	-	-
Au/SiO_2@mSiO_2(IM)-H_2-300	7.1±1.1	0.025	1.0	8	51.6	59
Au/SiO_2@mSiO_2(DP)-H_2-300	8.5±1.6	0.025	2.0	4	49.9	114
Au/SiO_2@mSiO_2(DP)-H_2-300	8.5±1.6	0.025	4.0	4	54.0	123

[a] No by-product was detected and complete selectivity was achieved in all the cases.

As far as the effect of the catalyst dosage was concerned, the morpholine conversion slightly increased with increasing the catalyst dosage from 0.025 to 0.05 g, as indicated by Table 3. In contrast, if decreasing the catalyst dosage from 0.025 to 0.015 g, the morpholine conversion will significantly decreased. Therefore, the catalyst dosage of 0.025 g was preferred in this work. The more the catalyst dosage, the more the active sites from the catalyst. As a result, the enlarged reaction opportunity was provided.

Correlation of morpholine conversion with reaction time was also investigated. As shown in Table 3, very low morpholine conversion was achieved at the reaction time of 1 h. The morpholine conversion can reach about 53.9% at the reaction time of 4 h. However, if further prolonging the reaction time to 8 h, the morpholine conversion little changed. Hence, the reaction time of 4 h was settled in this work. The effect of the quantity of H_2O_2 on morpholine conversion using Au-SiO_2@mSiO_2(DP, H_2) as catalysts was also studied. It can be seen from Table 3 that morpholine

conversion did not increase significantly even doubling and quadrupling the H_2O_2 amount.

Recycle tests were conducted to assess the durability of the catalyst, since durability is an important parameter of heterogeneous catalysts. The used catalyst was recovered by centrifugation and washed with ethanol and DI water, then dried and reused for another reaction under the same conditions. As shown in Fig. 10, the morpholine conversion remained almost the same during five consecutive cycles, indicating the remarkable stability of the catalyst.

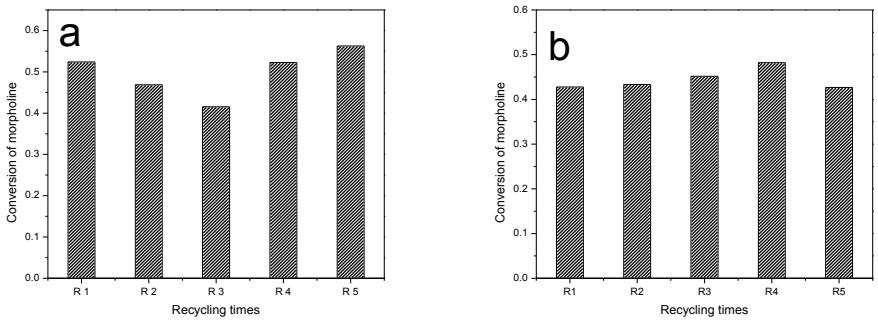

Figure 10 The catalytic performance of (a) Au-SiO_2@mSiO_2(DP)-H_2-300 ^oC and (b) Au-SiO_2@mSiO_2(IM)-H_2-300 ^oC catalysts for recycle and reuse.

Conclusions

In conclusion, core-shell silica comprising mesoporous SiO_2 shell and solid SiO_2 core (SiO_2@mSiO_2) was used as catalytic support to prepare Au/SiO_2@mSiO_2 catalysts for the reaction of benzaldehyde and morpholine. The high surface area of SiO_2@mSiO_2 was largely contributed by their mesoporous shell. As far as the IM method was concerned, more Au nanoparticles might be produced inside the mesopores in the shell of SiO_2@mSiO_2. For the DP method, the mesoporous shell was damaged to some extent. Furthermore, the formed Au nanoparticles were larger than those prepared by the IM method. The results also showed that the Au/SiO_2@mSiO_2 catalysts exhibited excellent catalytic activity and high durability. The morpholine conversion can reach about 53.9% while no side product was detected. Therefore, the as-prepared Au/SiO_2@mSiO_2 catalysts were

promising candidates for the reaction of benzaldehyde and morpholine.

Acknowledgements

The corresponding author greatly acknowledges for the financial support of Initiation Grant (Project No.: IGN12EG02) of the HKUST. This work is partially supported by the NSFC (Project No.21036004). J.H. is grateful to the Fujian Provincial Administration of Civil Service for the Fujian-Hong Kong joint postdoctoral fellowship. Rafael Luque gratefully acknowledges funding from MICINN under project CTQ2011-28954-C02-02 and Consejeria de Ciencia e Innovacion, Junta de Andalucia for funding project P10-FQM-6711. RL also kindly acknowledges the School of Engineering of Hong Kong University of Science and Technology, CBME and Prof. Guohua Chen for the provision of a Visiting Professorship in CBME, HKUST in 2013.

References

(1) T. Takei, T. Akita, I. Nakamura, T. Fujitani, M. Okumura, K. Okazaki, J.H. Huang, T. Ishida, M. Haruta, Heterogeneous Catalysis by Gold, *Advances in Catalysis*, Eds. B.C. Gates, F.C. Jentoft, 2012, Vol. 55, pp 1.

(2) M.C. Kung, R.J. Davis, H.H. Kung, *J. Phys. Chem. C* 2007, *111*, 11767.

(3) M.S. Chen, D.W. Goodman, *Acc. Chem. Res.* 2006, *39*, 739.

(4) M. Haruta, T. Kobayashi, H. Sano, N. Yamada, *Chem. Lett.* 1987, 405.

(5) M.S. Chen, D.W. Goodman, *Chem. Soc. Rev.* 2008, *37*, 1860.

(6) C.M. Friend, A.S.K. Hashmi, *Acc. Chem. Res.* 2014, *47*, 729.

(7) Y. Zhang, X. Cui, F. Shi, Y. Deng, *Chem. Rev.* 2011, *112*, 2467.

(8) A. Abad, P. Concepción, A. Corma, H. García, *Angew. Chem. Int. Ed.* 2005, *44*,

4066.

(9) G.W. Zhan, J.L. Huang, M.M. Du, D.H. Sun, I. Abdul-Rauf, W.S. Lin, Y.L. Hong, Q.B. Li, *Chem Eng J* 2012, *187*, 232.

(10) H. Yang, D. Tang, X. Lu, Y. Yuan, *J. Phys. Chem. C* 2009, *113*, 8186.

(11) M.M. Du, G.W. Zhan, X. Yang, H.X. Wang, W.S. Lin, Y. Zhou, J. Zhu, L. Lin, J.L. Huang, D.H. Sun, L.S. Jia, Q.B. Li, *J. Catal.* 2011, *283*, 192.

(12) X. Feng, X. Duan, G. Qian, X. Zhou, D. Chen, W. Yuan, *Appl. Catal. B* 2014, *150*, 396.

(13) X. Zhang, H. Shi, B.-Q. Xu, *Angew. Chem. Int. Ed.* 2005, *44*, 7132.

(14) X. Zhang, H. Shi, B.-Q. Xu, *J. Catal.* 2011, *279*, 75.

(15) A. Pineda, L. Gomez, A.M. Balu, V. Sebastian, M. Ojeda, M. Arruebo, A.A. Romero, J. Santamaria, R. Luque, *Green Chem.* 2013, 15, 2043.

(16) H.C. Zeng, *Acc. Chem. Res.* 2013, *46*, 226.

(17) W. Li, D. Zhao, *Adv. Mater.* 2013, *25*, 142.

(18) W. Stöber, A. Fink, E. Bohn, *J. Colloid Interf. Sci.* 1968, *26*, 62.

(19) H. Hamdan, M.N.M. Muhid, S. Endud, E. Listiorini, Z. Ramli, *J. Non-Crystalline Sol.* 1997, *211*, 126.

(20) T. Shimizu, T. Teranishi, S. Hasegawa, M. Miyake, *J. Phys. Chem. B* 2003, *107*, 2719.

(21) J.L. Huang, C. Liu, D. Sun, Y. Hong, M. Du, T. Odoom-Wubah, W. Fang, Q.B. Li, *Chem. Eng. J.* 2014, *235*, 215.